Magnetohydrodynamic instability of liquid and solid conductors. Destruction of conductors by an electric current

K. B. Abramova, N. A. Zlatin, and B. P. Peregud

A. F. Ioffe Physicotechnical Institute, USSR Academy of Sciences, Leningrad
(Submitted February 13, 1975)
Zh. Eksp. Teor. Fiz. **69**, 2007–2022 (December 1975)

The possible observation and identification of magnetohydrodynamic instabilities in solid and liquid cylindric conductors are discussed. Results are reported of an experimental study of the stability of liquid and solid conductors in the field of the current flowing through them. It is shown that the observed phenomena are satisfactorily described by the existing magnetohydrodynamic theory of stability of liquid and solid conductors in the field of their own current.

PACS numbers: 45.55.+e, 72.90.+y

Studies of the pinch effect in high-current electric discharges in gases were begun in the fifties, in the hope that they might lead to the realization of controlled thermonuclear fusion of light nuclei, and resulted in the discovery of a previously unknown phenomenon, namely, the instability of a plasma conductor in the field of the current flowing through it. The first theoretical papers devoted to the study of such instabilities, and the possible stabilization of current-carrying conductors, were published by Leontovich [1] and Leontovich and Shafranov. [2] The magnetohydrodynamic (MHD) description of the stability of a current-carrying plasma conductor was first used by Trubnikov [3] and Kruskal and Schwarzschild. [4] The most complete analysis of this problem has been given by Shafranov, [5-7] Tayler, [8,9] and Kadomtsev. [10] Important problems in this field have also been elucidated by a number of other authors. [11-13]

All the theoretical research in this field up to 1960, and most of the subsequent work, were stimulated by the thermonuclear problem, and the magnetohydrodynamic description was used as an approximation describing the behavior of a plasma conductor. The models of conductors which were employed took into account some of the properties (finite conductivity, but usually infinite viscosity [8]) and ignored other properties (low conductivity, surface tension) of the real conducting fluid. The compression of the plasma conductor by the field due to the current flowing through it (pinch effect), which can be neglected in liquid and solid conductors, was taken into account in a number of papers. [3,4,8,11] No attempt was made until 1960 to consider the behavior of real liquid conductors with finite (and low) conductivity and surface tension in the field of the current flowing through them, not to mention solid conductors with the attendant elastic characteristics.[1)] Moreover, in the first experimental work on MHD instabilities in liquid conductors, published by Dattner, Lehnert, and Lundquist, [14] and in the associated early theoretical work which took into account finite conductivity [9,15,16] and surface tension, [17-19] a jet of mercury was looked upon as an approximate model of a plasma conductor.

At the same time, the stability of liquid and, especially, solid conductors in electric and magnetic fields is, in our view, of independent scientific and great practical interest. In fact, to put it another way, it would be interesting to have an answer to the following question: what is the mechanism responsible for limiting the current flowing through a real superconductor, or a conductor with finite conductivity, and what is the magnitude of the limiting current? To avoid the trivial answer to this question, we shall suppose that the current flows through a nonsuperconductor for a time much shorter than that necessary to produce appreciable heating, and note that the critical current densities in superconducting compounds can now reach up to 10^7 A/cm^2 for a critical field of 10^4–10^5 Oe. [20] Departures from Ohm's law in metals may be expected for current densities of 10^9–10^{10} A/cm^2 [21] and, although it is obvious that to disrupt a solid conductor through the MHD instability the current must exceed some threshold value which, in turn, is determined by the strength parameters (see below), it is still reasonable to suppose that this threshold corresponds to current densities that are lower than those quoted above. It is expected that, in the not too distant future, the transmission of electric power will be based on the use of low-temperature or even moderate-temperature superconductors. When this situation is reached, the role of MHD phenomena in solid conductors will be difficult to overestimate.[2)]

In this paper, we consider the possibility of observing MHD instabilities in liquid and solid conductors, and of obtaining quantitative results. We also present some experimental results which are compared with theoretical calculations.

OBSERVATION AND MEASUREMENT OF MHD INSTABILITIES IN LIQUID AND SOLID CONDUCTORS. DEMANDS ON THE THEORY

Instabilities in liquid conductors can be observed by passing a current through jets of liquid metals, electrolytes, and metal-ammonia solutions which are known to exhibit metallic conductivity. The instability of solid conductors can be observed by passing high-density ($j > 10^5$ A/cm^2) current pulses through metal conductors. The pulse length must be short enough to ensure that the energy introduced into the conductor while the current pulse is flowing through it does not result in an appreciable change in the strength characteristics of the metal. Unless this condition is observed, quantitative results are subject to uncertainty which, naturally, impede comparison with theoretical predictions. In the process which is usually described as electric explosion, one can observe the development of MHD instabilities in both solid and liquid conductors, but reliable quantitative results, suitable for comparison with calculations, can be obtained only for instability modes developing in the conductor after transition to the liquid phase.

In solid conductors, MHD instabilities can be investigated in the case of a very pronounced skin effect, provided the pulse length is small in comparison with the time taken by the current to penetrate to an appreciable depth. Under these conditions, the interior of the conductor remains unheated in the course of the process (see [22] for more details) and the thickness of the molten layer can be calculated. [22,23]

In an experimental investigation of MHD instabilities, the following quantities can be compared with theoretical predictions: (1) threshold values of total current or current density corresponding to the appearance of particular instability modes and wavelengths, (2) the deformation rise time, (3) the spectrum of instability wavelengths and, in particular, the wavelength for which the growth rate is a maximum, and (4) the influence of external conditions and, above all, of the magnetic field, on instability development.

It is desirable that theoretical calculations used to interpret experimental results should take into account surface tension, finite conductivity, viscosity, and the strength parameters of the conductors. Moreover, they should be based on distributions of the electric and magnetic fields (intrinsic and external magnetic-field distributions over the cross section of the conductor) that are close to the distributions prevailing under the experimental conditions. Of course, the importance of allowing for any particular parameter depends on the particular conditions.

MHD INSTABILITIES OF LIQUID CONDUCTORS

It was shown in 1965–1966 [24-27] that MHD instabilities could be observed and play a dominant role, in processes developing during the passage of high-density current pulses through thin and initially solid conductors. Here, the problem is to show that, for a certain finite time, the current flows along a liquid conductor that retains the original form (but not the size) of the solid conductor, and that the conductor disintegrates when it is in the liquid phase.

As already noted, [24,25] there is a threshold value E_{th} of the total energy introduced by the current into the conductor, which separates the two possible but phenomenologically very different processes. In both cases, the passage of the current results in the dispersion of the conductor which "vanishes" but, for $E_{in} < E_{th}$, this occurs smoothly without any striking effect whereas, for $E_{in} > E_{th}$, the process is explosive in character and is accompanied by all the phenomena characteristic of an explosion, namely, a burst of sound, a shock wave, and a flash of light.[3)] The transition from the one stage to the other is most readily observed by recording the total radiation accompanying the process, integrated over the visible part of the spectrum (any other phenomenon can also be used). The two pairs of oscillograms in Fig. 1 show the current and the emitted radiation. They can be used to judge the difference between these two states, and to establish how critical is the threshold value of the energy: the energies introduced into the process differ by less than 10% and the applied voltages by less than 4%.

Table I lists the threshold energies E_{th} for conductors made of different metals. It is no accident that the table gives not the specific energies but the measured energies, since we are reluctant to regard the threshold energy as having a universal significance because its specific value should (and does) depend on, for example, the radius of the conductor. The essential point is that the threshold energy is always greater than the energy E_{melt} necessary to melt the conductor, and is less than the energy E_{evap} necessary to heat the conductor up to the evaporation temperature. This means that during the explosive stage the current flows through a liquid conductor for a time which depends on the current itself.

Figure 2 shows current and voltage oscillograms for three characteristic post-threshold cases. Transition from the one to the other is achieved by varying the applied potential difference, other conditions being held constant. These cases differ only by the presence or absence of a current pause. In the first case, the current ceases to flow after the disintegration of the conductor, and a high potential difference ($\sim 0.75U_i$) persists across the gap because the energy stored in the current source (a capacitor bank C_b) has not been exhausted. In the second case, the current stops flowing after the first pulse, but an arc discharge is produced after a certain period of time, the current flows again, and the capacitor bank is fully discharged. Finally, in the third case, the current pause has no time to develop, and the current curve shows the presence of only a dip which is followed by an arc discharge. At the instant of disintegration, the reaction of the electric circuit on the gap results in an overvoltage which very substantially exceeds the initial voltage across the capacitor bank. Oscillographs of this kind can be used to determine the amount of energy introduced into the process up to any particular instant of time, and to calculate, for example, the beginning and the end of the melting process. These two points are indicated by the arrows in Fig. 2. It is clear that, for a certain interval of time, the current flows through the liquid conductor, and the latter disintegrates after transition to the liquid phase.

It is possible to determine the behavior of the liquid conductor during the disintegration process by x-ray shadow photography, [24-27] but quantitative results can be obtained only in the case of high enough spatial and temporal resolution. Adequate spatial resolution will ensure that changes in the density of the material comprising

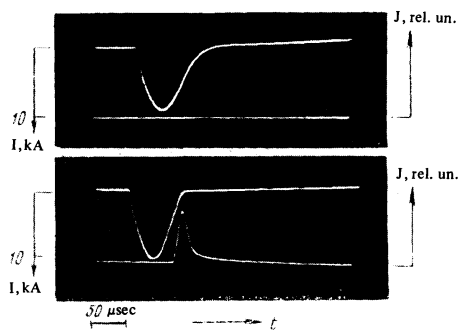

FIG. 1. Oscillogram showing the current I through the conductor and the light intensity J accompanying the explosion (λ = 2200-6000Å, Cu, r = 0.25 mm, l = 70 mm, C_b = 400 μF). Upper traces–U_i = 1150 V, E_{in} = 265 J; lower traces–U_i = 1200 V, E_{in} = 288 J.

TABLE I

Material	Diameter, mm	Length, mm	E_{melt}, J	E_{evap}, J	E_{th}, J
Cu	0.5	70	80	620	200
Pb	1.0	70	40	600	130
W	0.5	70	200	1620	250
Mo	0.5	70	150	935	180

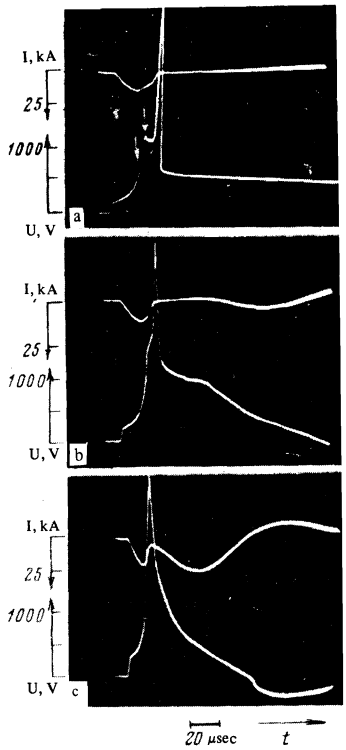

FIG. 2. Oscillograms showing the current I through the conductor and the voltage U across it (Cu, r = 0.25 mm, l = 70 mm, C_b = 2000 μF). Arrows on the upper voltage oscillogram indicate times at which the energy input is sufficient to start the melting process and to complete it. Initial voltage across the capacitors: a—1 kV; b—2 kV; c—3 kV.

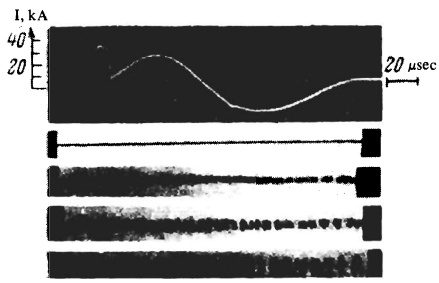

FIG. 3. X-ray shadow photographs of a copper conductor in the process of disintegration. Exposure 80 nsec. Conductor length 70 mm; $E_{in} > E_{th}$. Bars on the current oscillograms show the times at which the photographs were taken.

the conductor can be recorded at distances smaller than its diameter. The x-ray pulse length should be substantially less than the current decay time (in the case of the oscillograms reproduced here, not more than 100 nsec [29]).

Figure 3 shows examples of x-ray shadow photographs of liquid conductors (post-threshold state) in the course of disintegration. The instability producing the disintegration of the conductor can be clearly seen in the photographs.

Oscillograms and photographs similar to those reproduced in Figs. 2 and 3 can be used to determine at least two of the quantities listed above, namely, the time of instability development and its wavelength corresponding to maximum growth rate, and to compare them with theoretical predictions. Before we do this, let us briefly review the theoretical results reported in the papers mentioned above. We shall be largely concerned with the results for sharply bounded, incompressible liquid conductors, carrying currents distributed uniformly over their cross section, which have been obtained with allowance for finite conductivity and surface tension forces.[4)]

Analysis of the behavior of the conductor involves an analysis of the stability of solutions of the MHD equations (usually by the method of small perturbations). The complete set of magnetohydrodynamic equations relating the pressure p, the density ρ, and the velocity v of the medium carrying the current of density j in electric and magnetic fields E and H, includes the field equations, i.e., the Maxwell equations (the displacement current is neglected), Ohm's law for the moving medium, and the equations of hydrodynamics, i.e., the equations of motion and the equation of continuity. Perturbations of the equilibrium configuration, i.e., increments of any particular variables under perturbation, are assumed to be small. For example, if the shape of a cylindric conductor is altered so that its surface assumes the form

$$r = r_0 + \xi(z, \varphi, t), \tag{1}$$

where r_0 is the radius of the conductor in the equilibrium state and $\xi(z, \varphi, t)$ is an arbitrary function of cylindric coordinates and of time, then it is assumed that

$$\xi \ll r_0. \tag{2}$$

This enables us to linearize the equations, write the total perturbation as a superposition of waves of the form

$$\xi(z, \varphi, t) = \sum_{k,m} \xi_{k,m} \exp\{i(kz + m\varphi + \omega t)\} \tag{3}$$

and consider the instability separately for each perturbation with wave number $k = 2\pi/\lambda$ and azimuthal wave number m = 0, 1, 2, 3 ... . It is convenient to express the wavelength in units of the radius by substituting $x = kr_0$.

The zeroth mode (m = 0) is an axially symmetric sausage-type perturbation. The first mode (m = 1) corresponds to the screw (kink) perturbation. Higher-mode perturbations (m > 1) do not lead to the curving of the axis of the conductor, but produce a change in the shape of its cross section and may even give rise to the splitting into filaments (see, for example, [5]). In the cases in which we are interested (uniformly distributed current, zero longitudinal magnetic field), higher-mode instabilities do not develop. [8,16,18]

The stability of the conductor can be determined by establishing whether the quantity ω^2 is positive or negative. The stability condition is $\omega^2 > 0$. To obtain quantitative relationships for the growth rate of a perturbation ω as a function of the mode number m, wavelength x, conductivity σ, density ρ, surface tension α,[5)] the initial radius of the conductor, and the current, we must derive and solve the dispersion relation.

The method of deriving the dispersion relation for the cases in which we are interested was developed by a number of workers. [8,9,15,18,19]

In certain special cases, the dispersion equation can be solved by introducing various simplifying assumptions. Quite frequently, analysis of the dispersion equation yields the boundaries of the stability region, and certain other conclusions on the behavior of the growth rate, so that it is always possible to achieve numerical results. This was used in [24-27], where the dimensionless growth rate

$$\Omega = i\omega r_0 (4\pi\rho)^{1/2}/H_0 \qquad (4)$$

was calculated as a function of $x = kr_0$ for m = 0, m = 1, and different values of the dimensionless parameters q and f which depend on conductivity, density, and surface tension:

$$q^2 = \frac{r_0\sigma|H_0|}{c^2}\left(\frac{4\pi}{\rho}\right)^{1/2}, \quad f = \frac{4\pi\alpha}{r_0 H_0^2}. \qquad (5)$$

In these expressions, $H_0 = 0.2I/r_0$ is the intensity due to the current I (in amperes), flowing on the undisturbed surface of the conductor. All the other quantities are given in cgs esu.

Figure 4 shows the results of the calculations. For relatively large values of f, the growth rate reaches its maximum value within the confines of the graph. The growth rate is always zero for x = 0 and for a certain value $x = x_0$ (usually, $x_0 > 1$). The growth rate reaches its maximum within the interval $0 < x < x_0$. For $x \gg 1$, we have the asymptotic formulas:

$$\Omega^2 \approx 2(1 - 1/2x + \ldots) - x^3 f \quad \text{for } m = 0, \qquad (6)$$

$$\Omega^2 \approx 2(1 - 2m^2/x + \ldots) - x^3 f \quad \text{for } m \geq 1. \qquad (7)$$

It follows from (6) and (7) that, for large values of x, the maximum growth rate, $\Omega_{max} = \sqrt{2}$, is reached for

$$x = (3f)^{-1/3} \quad (m = 0), \qquad (8)$$

$$x = (4m^2/3f)^{1/4} \quad (m \geq 1). \qquad (9)$$

As far back as 1964, Gupta [19] showed that this behavior of the growth rate ($\Omega = 0$ for $x = x_0$) was connected with surface tension forces, whereas when these forces were ignored Ω tended asymptotically to a constant value as $x \to \infty$ even when finite conductivity was taken into account. [9] 6)

The foregoing results enable us to determine the perturbation wavelength corresponding to Ω_{max} and the time constant of the development of this perturbation

$$\tau_{theor} = \frac{r_0(4\pi\rho)^{1/2}}{H_0\Omega_{max}}. \qquad (10)$$

These parameters can be compared with measured values. The simplest procedure is to take two x-ray photographs, one of which shows the conductor still intact and the other the onset of periodic breaks along the length of the conductor (Fig. 3), and take the time interval between the two photographs as the experimental instability development time. Since the instability development time up to the complete disintegration of the conductor, t_{exp}, should be greater than one time constant, t_{exp} should be greater than τ_{calc}. This is, in fact, confirmed by the data shown in Table II. Despite the very considerable uncertainties in t_{exp}, comparison shows that the results are very satisfactory, especially insofar as the dependence of t_{exp} on current, diameter, and the material of the conductor is concerned.

Let us now compare the experimental and theoretical wavelengths of the developing instabilities. In the foregoing discussion, we were concerned with sausage-type instability (m = 0) although Eq. (10) and Fig. 4 indicate that the maximum growth rates for the two modes (m = 0 and m = 1) are the same. The justification for assuming that, in this case, we are concerned with the m = 0 mode is that the conductor disintegrates and the current ceases. The kink instability (m = 1) cannot result in the disintegration of the conductor when it develops to an amplitude of the order of r_0, and cannot be visually distinguished against the sausage-type instability background on the x-ray photographs.

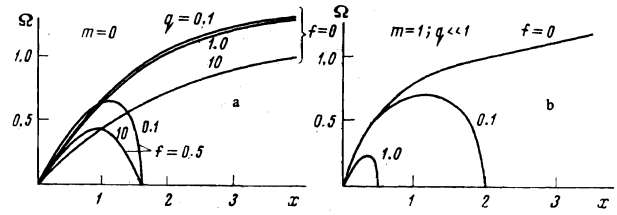

FIG. 4. Dimensionless growth rate $\Omega = i\omega r_0(4\pi\rho)^{1/2}H_0$ for m = 0 (a) and m = 1(b) as a function of the reciprocal of the dimensionless wavelength $x = 2\pi r_0/\lambda$.

TABLE II

No.	Material	r_0, mm	r_1, mm	I_{max}, kA	τ_{calc}, sec	λ_{calc}, mm	λ_{calc}, mm	λ_{exp}, mm	t_{exp}, sec	Notes
1	Cu	0.25	0.33	50	0.47	1	0.10	0.14		Conductor length 70 mm
2		0.25	0.34	50	0.47	2	0.10	0.17; 0.33; 0.65	1.5	α = 453 dyne/cm [20]
3		0.25	0.37	50	0.47	1	0.12	0.39; 0.52	2.9	ρ_{Cu} = 8.9 g × cm^{-3}
4		0.25	0.38	36	0.65	6	0.14	0.17; 0.55	4.0	σ_{Cu} = 0.645 × 10^6
5		0.25	0.38	33	0 8	2	0.15	0.14; 0.38		(Ω × cm)$^{-1}$
6	Pb	0.50	0.60	25	5.9	6	0 30	0.33	2.0	ρ_{Pb}=11.4,
7		0.50*	0.50	16	6.6	6	0.30	0.32		σ_{Pb}=0.053·10^6
8	W	0.25	0.34	12	5 6	12	0.22	0.22; 0.24; 0.50	1 8	ρ_W=19.3
9		0.25	0.43	10	10	12	0.32	0.47		σ_W=0.2·10^6
10		0.15	0.23	7	5.0	18	0.17	0.69		
11		0.15	0.27	10	4.4	18	0.21	0.42		
12	Mo	0.25	0.28	12	6	10	0.16	0.35		ρ_{Mo}=10.2,
13		0.25	0.37	10	8	6	0.27	0.37		σ_{Mo}=0.194·10^6

*Explosion of liquid lead.

Our task now is to compare the measured wavelength of a highly developed instability with the calculated wavelength $\lambda_{\Omega max}$ corresponding to the maximum growth rate. This can be done with the aid of x-ray photographs similar to those reproduced in Fig. 3. There are, however, certain complicating factors. For the experiments which we are considering, the parameter f is always substantially less than unity, and this means that (see Fig. 4a) $\Omega = \Omega(x)$ is a very slowly-varying function. The isolation of the instability with $\lambda_{\Omega max}$ against the background of oscillations with other wavelengths will therefore necessarily occupy an appreciable amount of time. Moreover, one must use photographs referring to instants of time lying as close as possible to the onset of instability development. This requirement is dictated by the fact that arc discharges develop in the constrictions as soon as the first breaks appear in the conductor. These arcs produce high-density vapor which masks the structure of the liquid conductor on the photographs. They also result in a reduced thickness of the disks (or even the total disappearance of individual disks) and hence to an increase in the length of the gaps between them. This in turn may distort measurements of $\lambda_{\Omega max}$.

The solution is to use x-ray photographs of the conductor at a relatively early stage of instability development, and to perform a Fourier analysis of the corresponding microdensitometer curve (image density as a function of position along the conductor) with a view to isolating the harmonic with the maximum amplitude. The result obtained by dividing the length l of the conductor by the number N of constrictions within this length is quite unsuitable for comparison with the theoretical value of l/N.

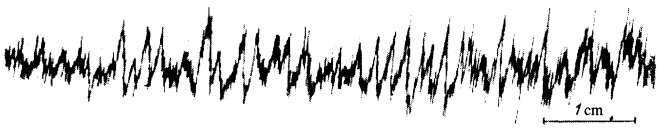

FIG. 5. Microdensitometry of an x-ray shadow photograph of an explosion of a copper conductor.

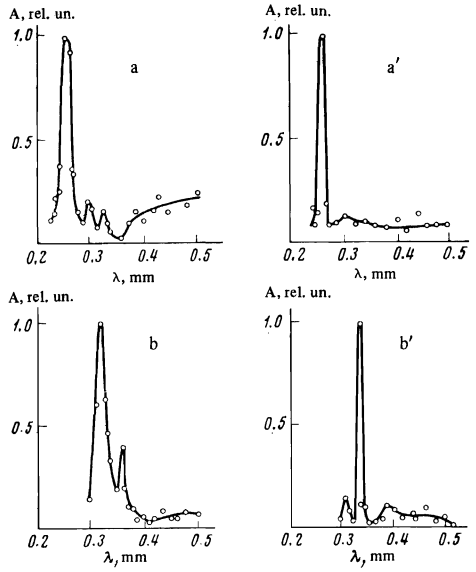

FIG. 6. Plots of A(λ) normalized to unity.

A typical microdensitometer trace is shown in Fig. 5. The result of the Fourier analysis of such curves can be given in the form of the amplitude A as a function of either the number n of the harmonic or the wavelength λ (Fig. 6). During the early stages of the process, the spectrum consists of a large number of harmonics, as expected, but there is always a harmonic $\lambda_{A\max}$ which is clearly different from all the others and occurs near the calculated value (a total of 20 cases was analyzed). Table II summarizes the conditions under which the experiments were performed, and lists the values of $\lambda_{A\max}$ and $\lambda_{\Omega\max}$. The agreement between the experimental and calculated values of λ is found to be satisfactory. In several cases, the spectrum contains long-wavelength harmonics. Values of these wavelengths, λ^{l}_{exp}, are also listed in Table II (see below for an explanation of their origin).

Figures 6a and 6a′ show the spectra for $f = 10^{-5}$, $q = 0.3$ (this corresponds approximately to lead), and $r_0 = 0.5$ mm for two arbitrarily chosen values of the dimensionless time $t' = \omega_{\max} t$. These spectra were obtained by precisely the same method as was used in the analysis of the microdensitometer curves but, in this case, we analyzed the calculated generator of the cylinder whose surface was formed under the action of the developing instabilities.[7)] Figures 6b and 6b′ show, respectively, the instability spectrum for a jet of liquid lead at the time approaching current cutoff, and a subsequent instability spectrum for an initially solid lead conductor.

Comparison of the spectra corresponding to the early (Fig. 6a, b) and later (Fig. 6a′, b′) instants of time clearly illustrates the evolution of these spectra. Comparison of the results of an analysis of curves known to consist of a large number of harmonics, developing with the corresponding growth rates (Fig. 6a, a′), with the results of an analysis of the experimental results (Fig. 6b, b′) enables us to conclude that the procedure which we have used does, in fact, reveal the presence of the harmonic corresponding to the maximum growth rate.

In conclusion, we note that comparison of the experimental results with the MHD theory of stability of liquid conductors in the field of the current flowing through them shows that the MHD theory can be used to predict the behavior of liquid-metal conductors in a broad range of current densities and conductor parameters to an accuracy sufficient for practical purposes.

MHD INSTABILITY OF SOLID CONDUCTORS

Less well-known from the practical point of view, but evidently more interesting than the case considered in the preceding section, are the instabilities which appear and develop in solid conductors. The first theoretical paper (1962) on the stability of a solid cylindrical rod in the field of its own current is due to Dolbin [31]. The conductivity of the rod was assumed to be infinite, and the current was therefore a surface current. A dispersion relation was derived and some numerical calculations were made for m = 0 perturbations. This illustrated the behavior of the growth rate as a function of the current, the strength properties of the conductor, and the perturbation wavelength. Asymptotic expressions were obtained for short-wave ($x \to \infty$) and long-wave ($x \to 0$) oscillations with m = 0, including, in particular, the dependence of the threshold current on the elastic parameters (for $x \to 0$). The threshold current was calculated as a function of the perturbation wavelength for m = 0.

Dolbin and Morozov [32] investigated the elastic long-wave ($x \ll 1$) kink (m = 1) oscillations of a rod of circular and elliptic cross section in the case of infinite conductivity (surface current). A dispersion relation and a stability condition were obtained for such rods, the latter in the form of the maximum current for which the rod was still stable.

Vandakurov and Kolesnikova [33] reported their results in 1967. They were obtained sometime before that date in connection with the first reports of experimental work on the stability of solid conductors.[24,25] Vandakurov and Kolesnikova [33] investigated the conditions for the appearance of instability in a solid cylindric conductor of poor conductivity, $q \ll 1$ [see Eq. (5)], and obtained the following dispersion relation between ν^2 and the parameters m, x, h, and γ:

$$\nu = i\omega r_0 (\rho/\lambda)^{1/2}, \quad h = H_0^2/8\pi\lambda, \qquad \gamma = 2G/\lambda = 1/\mu - 2, \quad \Lambda = \mu E_Y/(1+\mu)(1-2\mu), \tag{11}$$

where G is the shear modulus, μ is Poisson's ratio, E_Y is Young's modulus, and $\Lambda + \frac{2}{3}G$ is the hydrostatic compression modulus. The dispersion relation was solved by a numerical method, and yielded curves showing ν as a function of the four parameters m, x, h, and γ. Under given conditions, these curves can be used to determine the instability development threshold, the minimum wavelength for a given current, or the wavelength for which ν is a maximum, and the instability growth time:

$$\tau_s = \frac{r_0}{\nu}\left[\frac{(1+\mu)(1-2\mu)\rho}{\mu E_Y}\right]^{1/2}. \tag{12}$$

As expected, there is a threshold current $I_{th}(h_{th})$ for both instability modes. Under given conditions (given μ,

E_Y, r_0), the instability will not develop provided $I < I_{th}$. The threshold current I_{th} for the sausage-type instability and constant other conditions is substantially greater than the threshold current for the screw instability: $I'_{th\,m=0} > I_{th\,m=1}$. Thus, for example, to excite the screw instability in a cold solid conductor, 0.5 mm in diameter and made from cold rolled copper (μ = 0.33, $E_Y = 1.2 \times 10^{12}$ dyne/cm^2) one needs a current greater than $\sim 2 \times 10^5$ A ($j = 10^8$ A/cm^2), whereas to excite the sausage-type instability, the current must be greater than 7×10^5 A ($j = 3.5 \times 10^8$ A/cm^2). It follows from the discussion in the last section (see also the discussion given below) that for currents of the order of 10^4 A ($j = 5 \times 10^6$ A/cm^2), the time spent by a conductor of this kind in the solid state is already smaller than the time necessary for instability development. The conductor rapidly melts and is destroyed by the instability that appears and develops in the liquid conductor. Nevertheless, screw instability in the solid conductor (when the energy introduced in one pulse is $E_{in} < E_{th}$) can readily be recorded and even noted visually: it is possible to ensure that the current flows through the conductor in the form of a pulse whose amplitude and length are such that the instability will develop but the conductor will not succeed in disintegrating. Instability development becomes possible because of the heating of the conductor by the current flowing through it. To ensure that the deformation is large enough (but the conductor does not disintegrate), the conductor must be "stretched" gradually by passing through it several current pulses. Figure 7 shows the photograph of a conductor with a "frozen" instability.

For large currents, when the conductor disintegrates but the process does not as yet resemble an explosion in any way ($E_{in} < E_{th}$),[8)] the instability can be recorded by x-ray photography of the conductor. Figure 8 gives an example of an x-ray photograph of this kind, showing a conductor both at the beginning of current flow and 350 μsec after the end of this flow. It is clear that segments of the conductor which are accelerated during the instability development process continue to move for a considerable time after the current has ceased to flow. At this stage, the conductor is already in the molten state because the energy introduced under these conditions can be both less than and greater than the energy necessary for melting. Individual segments of the conductor where, owing to the ever-present inhomogeneities in the shape and properties of the conductor, there is a considerable heat release, may even become vaporized under these conditions. This is clearly shown by the x-ray photographs. However, the onset of instability occurs (see below) in the still solid conductor. When the energy input E_{in} approaches the threshold value E_{th}, but is somewhat greater than the latter, it is also possible to observe both the screw instability in the solid conductor and the sausage-type instability which develops after the transition of the conductor to the liquid state.

It is implicitly assumed in the preceding section that no instabilities will develop in the post-threshold state until the conductor melts. In fact, because of the relatively long time constant of the process in the post-

FIG. 7. Photograph of a conductor with "frozen" instability.

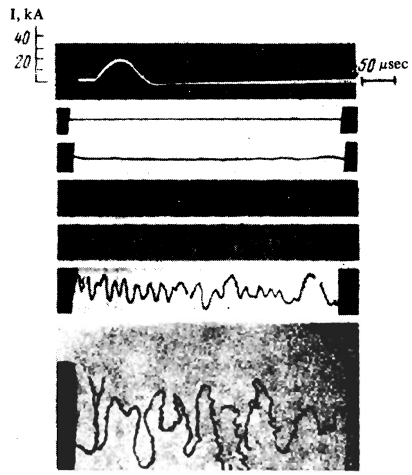

FIG. 8. Shadow x-ray photograph of a copper conductor in the process of disintegration. Bars on the current oscillogram show the times at which the photographs were taken, $E_{in} < E_{th}$.

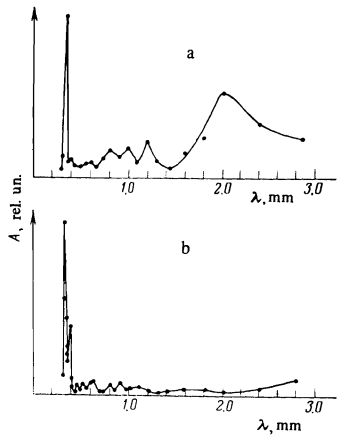

FIG. 9. Experimental instability spectra: a—PB(wire), r_0 = 0.50 mm, I = 25 kA, λ_{calc} = 0.30 mm (case 6, Table II); b—Pb(jet), r_0 = 0.50 mm, I = 16 kA, λ_{calc} = 0.30 mm (case 7, Table II).

threshold state ($E_{in} > E_{th}$), the instability will not succeed in developing in the solid conductor to the extent that it becomes readily distinguishable from that developing in the liquid conductor (visually on the x-ray photographs). However, this instability can be seen as a relatively long-wave phenomenon on the microdensitometer curves obtained for the x-ray photographs (see Fig. 5) (long-wave, that is, as compared with the sausage-type instability). Convincing evidence for the fact that the long-wave instability develops in the still solid conductor (and is therefore a screw instability) is provided by an experiment, the results of which are shown in Fig. 9. Other things being constant, if the conductor (Pb) is initially solid, the long-wave instability is well developed and, if it is initially in the liquid state (liquid lead jet), then the instability is absent.

Table III (columns 1—5) lists the experimental conditions in the subthreshold state, the results for which were subjected to numerical analysis. Column 8 gives the values of the parameter h_{cc} [see formula (11)], calculated for a cold conductor, and columns 9 and 10 give the values of the threshold parameter h_{th} for instabilities with m = 1 and m = 0. Comparison of these quantities shows that neither one nor the other instability can develop in the cold conductor. The instability (above all, the m = 1 mode) should begin to develop after the heating of the conductor by the current at the time when h_{hc} becomes equal to or somewhat greater than h_{th} due to the

TABLE III

Material	r_0, mm	E_Y, dyn/cm², $T = 20°C$	T, $\mu = 20°$ C	I_{max}, A experiment	I_{th}, A calc, m = 1	h_{th} calc, m = 1	h_{cc}	h_{th} calc, m = 1	h_{th}, calc, m = 0
1	2	3	4	5	6	7	8	9	10
Pb	0,5	$0.18 \cdot 10^{12}$	0,45	$7 \cdot 10^3$	$8 \cdot 10^4$	$3 \cdot 10^5$	$5,8 \cdot 10^{-4}$	$\sim 10^{-2}$	0,14
Cu	0.25	$1.2 \cdot 10^{12}$	0,33	$18 \cdot 10^3$	$1.9 \cdot 10^5$	$7 \cdot 10^5$	$9.0 \cdot 10^{-4}$	$\sim 10^{-1}$	1.5
W	0.25	$3.5 \cdot 10^{12}$	0.28	$9 \cdot 10^3$	$1.6 \cdot 10^5$	$1.5 \cdot 10^6$	$1.2 \cdot 10^{-4}$	$4 \cdot 10^{-2}$	2.25

Material	λ_{exp}, mm	λ_{γ}, calc, m = 1	$x = 2\pi r_0/\lambda_{exp}$	h_{hc}	E_Y/E_{eff}	$\frac{E_{YO}}{E_{eff}}$	t_{exp}, μsec	τ_{hc}, μsec, calc	τ_{γ}, μsec, calc, m = 1
1	11	12	13	14	15	16	17	18	19
Pb	10	0.2	0.34	0.02	$4.8 \cdot 10^9$	37		100	1.5
Cu	2.5	0.1	0.6	0.2	$3 \cdot 10^9$	400	6	5.6	1.2
W	6	0.08	0.26	0.05	$2.4 \cdot 10^9$	700	15	50	3.1

reduction in E_{el}. For convenience, columns 6 and 7 give the threshold currents.

Since the instability develops in a highly heated conductor, its quantitative description requires the introduction of an arbitrarily chosen effective modulus E_{eff}. However, it is more natural to proceed as follows: the measured m = 1 instability wavelength is used in conjunction with the graph given by Vandakurov and Kolesnikova [33] to determine the parameter h_{hc} for which the instability does in fact occur, and the result is compared with h_{th} for m = 1. The wavelength λ_{exp} averaged over the length of the conductor was determined from the x-ray photograph corresponding to the instant of time at which the instability was first recorded with the current flowing through the conductor. Poisson's ratio was assumed to be independent of temperature. In some cases, the curves given in [33] had to be extrapolated to low values of h in order to determine the parameter h_{hc}. The values of h_{hc} found in this way (column 14) are in good agreement with the expected values: $h_{hc} \gtrsim h_{th}$ for m = 1 (column 9).

The value of h_{hc} can be used to determine E_{eff} (column 15). It is interesting that E_{eff} is roughly the same for all the cases, whereas the corresponding E_Y differ by factors of 20. Finally, if we know $x = 2\pi r_0/\lambda_{exp}$ and E_{eff}, we can use the functional relationship $\nu(x)$ given in [33] to determine the growth rate ν and to calculate the instability rise time τ_{hc} for an instability of given wavelength. The instability development time t_{exp} was assumed to be equal to the time between two x-ray photographs, the first of which shows the undeformed conductor and the second clearly indicates the presence of instability. The values of t_{exp} and the calculated τ_{hc} are listed in columns 17 and 18 of Table III.

Comparison of λ_{exp} and t_{exp} with the corresponding calculated values for a liquid conductor (columns 12 and 19 in Table III) once again shows that these instabilities do appear in the solid conductor.

The foregoing quantitative comparison between experimental and calculated results, although it is more approximate than in the case of liquid conductors, does nevertheless appear to identify reliably the observed phenomena, but also enables us to conclude that existing theory provides a satisfactory description of the observed phenomena.

MHD instabilities in solid conductors under more definite conditions can be investigated either in the above case of a strong skin effect or in conductors prepared from superconducting compounds.

The authors are indebted to Yu. V. Vandakurov for fruitful discussions and to K. A. Aristova for her participation in the present investigations.

[1)] In general, the situation in the case of solid conductors is no longer "hydrodynamic," but we shall continue to use this word in the absence of other suitable terminology.

[2)] This was brought to our attention by A. I. Morozov.

[3)] In the subthreshold state, radiation is also emitted but is confined to the infrared region. See [28] for more details regarding this radiation.

[4)] Careful analysis has shown that in our experiments, and in all the experiments known to us, which involve the passage of high-density currents through conductors, including in particular all papers on electric explosions, the skin effect is practically absent because, usually, the shorter the current pulse, the thinner is the conductor used in the experiments.

[5)] In the calculations reported here, the quantities σ, ρ, and α are assumed to be constant during the instability development.

[6)] When $\dot{\sigma} = \infty$, we have $\Omega \to \infty$ ($\lambda \to 0$) for $\chi \to \infty$ ($\lambda \to 0$). [8]

[7)] To determine the instability spectra at times approaching the onset of instability development, we must take into account the possible development of instabilities with wavelengths corresponding to the entire range covered by the function(x): from x = 0 to $x = x_{\Omega=0}$. The generator of the cylinder was calculated on a computer for the selected instant of time, using the formula

$$r = r_0 + B \sum_{\eta_1}^{\eta} \exp\left(\frac{\Omega_\eta t'}{\Omega_{max}}\right) \sin\frac{2\pi r_0}{l} \eta_k \xi_i$$

on the assumption that the appearance of the initial perturbations is equally probable for all wavelengths. In this expression, η is the number of values of x for which $\Omega(x)$ was calculated (we chose $\eta = 1200$) and ξ is the number of points at which r was calculated ($\xi = 100$).

[8)] Here again, the threshold value of the energy introduced into the conductor is the value which separates two very different stages, namely, the subthreshold stage and the electrical explosion stage.

[1] M. A. Leontovich, in: Fizika plazmy i problema upravlyaemykh termoyadernykh reaktsiĭ (Physics of Plasma and the Problem of Controlled Thermonuclear Reactions), Vol. 1, AN SSSR, 1958, p. 110.

[2] M. A. Leontovich and V. D. Shafranov, in: Fizika plazmy i problema upravlyaemykh termoyadernykh reaktsiĭ (Physics of Plasma and the Problem of Controlled Thermonuclear Reactions), Vol. 1, AN SSSR, 1958, p. 207.

[3] B. A. Trubnikov, in: Fizika plazmy i problema upravlyaemykh termoyadernykh reaktsiĭ (Physics of Plasma and the Problem of Controlled Thermonuclear Reactions), Vol. 1, AN SSSR, 1958, p. 289.

[4] M. D. Kruskal and M. Schwarzschild, Proc. R. Soc. Ser. **A223**, 348 (1954).

[5] V. D. Shafranov, in: Fizika plazmy i problema upravlyaemykh termoyadernykh reaktsiĭ (Physics of Plasma and the Problem of Controlled Thermonuclear Reactions), Vol. 1, AN SSSR, 1958, p. 130.

[6] V. D. Shafranov, At. Énerg. 5, 38 (1956).

[7] V. D. Shafranov, in: Fizika plazmy i problema upravlenyaemykh termoyadernykh reaktsiĭ (Physics of Plasma and the Problem of Controlled Thermonuclear Reactions), Vol. 4, AN SSSR, 1958, p. 61.

[8] R. J. Tayler, Proc. Phys. Soc. London Ser. B **70**, 31 (1957); **70**, 1049 (1958).

[9] R. J. Tayler, Rev. Mod. Phys. **32**, 907 (1960).
[10] B. B. Kadomtsev, in: Voprosy teorii plazmy (Problems of Plasma Theory), Gosatomizdat, 1963, p. 132.
[11] T. F. Volkov, Sb. Fizika plazmy i problema upravlyaemykh termoyadernykh reaktsiĭ (Physics of Plasma and the Problem of Controlled Thermonuclear Reactions), Vol. 2, Izd. AN SSSR, 1958, p. 144.
[12] P. H. Roberts, Astrophys. J. **124**, 430 (1956).
[13] Yu. V. Vandakurov and K. A. Lur'e, Zh. Tekh. Fiz. **29**, 1170 (1959) [Sov. Phys.-Tech. Phys. **4**, 1068 (1960)].
[14] A. Dattner, B. Lehnert, and S. Lundquist, Second United Nations Intern. Conf. on the Peaceful Uses of Atomic Energy, P/1708, 1958.
[15] S. N. Breus, Zh. Tekh. Fiz. **30**, 1030 (1960) [Sov. Phys.-Tech. Phys. **5**, 960 (1961)].
[16] Yu. V. Vandakurov, Zh. Tekh. Fiz. **33**, 145 (1963) [Sov. Phys.-Tech. Phys. **8**, 104 (1963)].
[17] G. S. Murty, Ark. Fys. **18**, 241 (1960).
[18] G. S. Murty, Ark. Fys. **19**, 483 (1961).
[19] A. S. Gupta, Proc. R. Soc. Ser. A **278** 80 (1964).
[20] C. P. Bean, R. L. Fleischer, P. S. Swartz, and H. R. Hart, J. Appl. Phys. **37**, 2218 (1966).
[21] E. M. Purcell, Electricity and Magnetism (Russ. Transl.), Nauka, 1971.
[22] M. L. Lev, B. P. Peregud, and Z. V. Fedichkina, Zh. Tekh. Fiz. **45**, No. 12 (1975) [Sov. Phys.-Tech. Phys. **20**, No. 12 (1976)].
[23] A. I. Gubanov, Zh. Tekh. Fiz. **43**, 2023 (1973) [Sov. Phys.-Tech. Phys. **18**, 1277 (1974)].
[24] K. B. Abramova, V. P. Valitskii, Yu. V. Vandakurov, N. A. Zlatin, and B. P. Peregood, Phys. Lett. **18**, 286 (1965).
[25] K. B. Abramova, V. P. Valitskii, Yu. V. Vandakurov, N. A. Zlatin, and B. P. Peregood, Proc. Seventh Intern. Conf. Ion. Phen. in Gases, Belgrade, 1965.
[26] K. B. Abramova, V. P. Valitskiĭ, Yu. V. Vandakurov, N. A. Zlatin, and B. P. Peregud, Dokl. Akad. Nauk SSSR **167**, 778 (1966) [Sov. Phys.-Dokl. **11**, 301 (1966)].
[27] K. B. Abramova, Dissertation, A. F. Ioffe Physicotechnical Institute, Leningrad, 1969.
[28] K. B. Abramova and B. P. Peregud, Zh. Tekh. Fiz. **41**, 2216 (1971) [Sov. Phys.-Tech. Phys. **16**, 1758 (1971)].
[29] N. A. Zlatin and G. S. Pugachev, Zh. Tekh. Fiz. **40**, 2248 (1970) [Sov. Phys.-Tech. Phys. **15**, 1754 (1971)].
[30] D. P. Wilson, Structure of Liquid Metals and Alloys (Russ. Transl., Metallurgiya, 1972).
[31] N. I. Dolbin, Zh. Prikl. Mekh. Tekh. Fiz. **2**, 106 (1962).
[32] N. I. Dolbin and A. I. Morozov, Zh. Prikl. Mekh. Tekh. Fiz. **3**, 97 (1966).
[33] Yu. V. Vandakurov and É. N. Kolesnikova, Zh. Tekh. Fiz. **37**, 1984 (1967) [Sov. Phys.-Tech. Phys. **12**, 1458 (1968)].

Translated by S. Chomet
216